

Revised: November 20, 2018

# An Inverse Problem Approach to Cluster Dynamics

Dalia Chakrabarty<sup>1</sup>

*Department of Physics & Astronomy  
Rutgers University  
136 Frelinghuysen Road  
Piscataway, NJ 08854-8019, USA*

Simon Portegies Zwart

*Astronomical Institute 'Anton Pannekoek' and Dept. of Computer Science  
University of Amsterdam  
Kruislaan 403 1098SJ  
Amsterdam, the Netherlands*

## ABSTRACT

We propose a new non-parametric algorithm that can be implemented to study and characterize stellar clusters. The scheme attempts to simultaneously recover the stellar distribution function and the cluster potential by using projected radii and velocity information about the cluster members. The pair of these functions that is most consistent with the input data is detected by the Metropolis algorithm. In this work, the cluster characteristics recovered by CHASSIS are calibrated against the N-body realizations of two clusters, namely Hyades and Arches. The cluster mass and line-of-sight projected velocity dispersion profiles are correctly reproduced by the algorithm when the cluster obeys the assumption used in the code, namely isotropy in phase space. The results recovered by the code are shown to be insensitive to the choice of the initial parameters. The results are also not influenced by increasing the number of input data points as long as this number exceeds a minimum value which is moderately low for an input data set that obeys the assumptions of isotropy and sphericity.

*Subject headings:* Galaxy: center; Galaxy: kinematics and dynamics

## 1. Introduction

The characterization of stellar clusters is more often than not, an exercise in model building. One usually begins with an assumption (of sphericity) for the cluster geometry. Quite often, luminosity

measurements are used in conjunction with fitting algorithms to provide the surface brightness profile of the cluster (Larsen et al. 2001). However, a major shortcoming of such a procedure is that such fits are often unstable over the whole radial range considered. Moreover, the robustness of these fitting techniques is always challenged by details in the observed data. It is possible in principle to obtain smooth approximations to the surface density profile and projected velocity dispersion profiles from observations. These projected quantities could be inverted to yield their total or three dimensional counterparts via the Abel integral equation; such a deprojection is unique in the spherical case. Unfortunately an inversion of this nature is highly sensitive to shot noise in the data bins. Genzel et al. (1996) acknowledge this problem and adopt the more secure alternative of starting with parametrized forms of the density and radial velocity dispersion profiles, which are projected back to observational space, while maintaining the search for those projected profiles that fit the observed result best. Such an inverse approach, whenever possible, is almost always the better option since it involves less errors. Frequently, a cluster is considered to be in virial equilibrium; velocity dispersion estimates or enclosed mass information are then extracted from the virial equation (Bosch et al. 2001; Ghez et al. 1998). A method that can substitute this assumption of a virialized cluster is certainly more satisfactory since observations alone cannot be sufficient to establish the validity of this conjecture.

This state of affairs can be improved upon by considering the inverse problem approach. It is indeed true that such a formalism demands a moderately large data set. Kinematic information about the members of a number of observed stellar clusters suffices to fulfill this requirement. In this paper, we propose a non-parametric technique which can be used for the characterization of stellar systems. The algorithm presented here has been used before (Chakrabarty & Saha 2001) for the estimation of the mass enclosed in the inner few parsecs of the Milky Way (hereafter Paper I). We refer to our scheme as CHASSIS, i.e. CHAracterization of Stellar Systems using a new Inverse Scheme.

This paper aims to advance the case of using CHASSIS in investigations of stellar clusters. In order to establish the resourcefulness of this code, we test our inverse algorithm on two simulated star clusters, which were placed at known distances and projected on a selected part of phase space. We present the results of analyzing these simulated star clusters with CHASSIS and then compare the results with the cluster simulations. This comparative exercise reflects the degree of robustness of the algorithm.

## 2. Initial conditions and calculations

As input for the simulations we adopt two clusters which we use as templates for the initial conditions. We call these models A (mimicking the Arches star cluster) and H (mimicking the Hyades star cluster, see Table 1).

The cluster simulations were performed in three steps: 1) initialization of the stellar system,

2) calculation of the evolution of the cluster to a certain time and 3) preparation of the simulated star cluster to use as input for the inverse algorithm.

Details about the Hyades (model H) and the global setup of the calculations of the Arches model (model A) are published (Portegies Zwart et al. 2001; Portegies Zwart et al. 2002). One ingredient of the Arches model that makes it different compared to previously performed N-body calculations is the inclusion of the external tidal field of the Galaxy and the frictional drag force on the bound cluster. As a result, the cluster spirals in from an initial distance of 6pc from the Galactic center to less than 2pc, in about a million years. The strong tidal field in model A causes this cluster to become strongly aspherical and elongated perpendicular to the line connecting the cluster with the Galactic center. However, CHASSIS works on the assumption of sphericity of the cluster, as is explained below. In the light of this obvious contradiction, the results obtained from the inverse algorithm for the Arches cluster were expected to be interesting. Model A was run on a GRAPE-6 and took about 188 CPU hours. Model H took about 55 hours on a single board GRAPE-4.

For the selected models, positions and velocities of all stars are calculated self consistently together with the evolution of the stars and binaries in the clusters. Calculations are performed using the starlab software environment (see <http://manybody.org>) and utilize the GRAPE-4 and GRAPE-6 special purpose computers (Makino et al. 1997). The simulations were stopped and ported to the inverse algorithm when the age of the cluster is about 1 million years for model A and about 400 million years for model H. For model H all the stars remaining in the cluster after 400 million years were ported to the inverse algorithm while for model A the stars remaining after 1 million years were used. From these sets various smaller data sets were selected for direct input into CHASSIS (see below).

## 2.1. Preparation of the clusters for the inverse algorithm

The stellar samples used as inputs in our algorithm are selected from the N-body data sets that describe the two clusters. We use kinematic data of a maximum of about 2600 stars belonging to Hyades in our work. The number of stars in Arches from which input data is chosen is much higher (about 55,000). The input files for the algorithm are prepared by choosing stars either at a random or by picking stars according to their luminosity. The kinematic information provided in the N-body data sets about each star is made to undergo appropriate transformations in order to calculate the corresponding apparent position, radial velocity and transverse velocity. These quantities are the inputs for our code CHASSIS. Diagrammatic representations of the kinematics of the two clusters are in Figure 1 and Figure 2. These are plots of radial and transverse velocities against radial positions of the stars on the plane of the sky, i.e. the apparent position of the stars.

The N-body simulations indicated that the clusters are neither isotropic, nor are they perfectly spherical. The extent of the presence of anisotropy and asphericity in the A and H models is brought

out in Figure 3 which displays the radial dependence of the ratios of the  $x$  and  $y$  components of the velocity dispersion vector ( $\sigma_{vx}$  and  $\sigma_{vy}$ ) to the  $z$  component of the same ( $\sigma_{vz}$ ) and the  $x$  and  $y$  component of the spatial dispersion vector ( $\sigma_x$  and  $\sigma_y$ ) to the  $z$  component of the same ( $\sigma_z$ ). Such ratios are only crude estimates of the deviation from sphericity and isotropy, but they serve our purpose of estimating the degree to which we can expect the input data to be incongruous with the assumptions of the code.

As can be seen from this figure, in the H-model, the ratios of the spatial dispersions is about 1 to a radius about 5pc, after which both  $\sigma_x/\sigma_z$  and  $\sigma_y/\sigma_z$  rise with radius slowly though a marked discontinuity in the run of the spatial dispersions shows up just inside a radius of about 10pc. A big jump occurs in the ratios  $\sigma_{vx}/\sigma_{vz}$  and  $\sigma_{vy}/\sigma_{vz}$  between about 4pc and 7pc. This picture prompts us to choose to work within about 10pc in the Hyades cluster, knowing that the kinematic distribution of this input data is not very well consistent with isotropy in this radial range.

The equivalent radial cutoff for the A-model appears to be about 0.2pc, though further on, the cluster gets highly aspherical and anisotropic. So we choose to select kinematic information of the A-model from radii within 0.2pc.; however when viewed at a finer resolution, even within this radius, the run of the dispersion ratios is quite jerky, indicating that the data from the Arches cluster does not abide by the assumptions of isotropy in the code.

The chosen radial ranges are also inclusive of the half-mass radii of the two clusters, about 4.66pc for Hyades and 0.093pc for Arches. From the H-model and the A-model, the mass enclosed within 4.6pc and 0.093pc are approximately  $584M_\odot$  and  $24522M_\odot$ , respectively. These mass values are very close to half the mass of the cluster (see Table 1).

### 3. Algorithm used

The code used in our work was introduced and discussed in details in Paper I. Observed kinematic data (apparent positions of stars on the plane of the sky and their velocities) is used as input in this algorithm. CHASSIS is a non-parametric code which attempts to identify both the equilibrium stellar distribution function (DF) from which the observed kinematical data is drawn as well as the potential of the observed stellar system. The code assumes sphericity of this stellar system. In its present form the scheme also assumes an isotropic DF. Paper I reports a test that was developed to check the consistency of the used data with the assumption of isotropy. The basic design of our algorithm is described briefly below.

As an initial guess, the code requires a set of functions in the form of an arbitrarily chosen trial potential ( $\Phi$ ) (rather the corresponding density profile  $\rho$ ) and distribution function  $f$ , which is a function of energy  $E$  only, via the assumption of isotropy. The final results have no bearing on the initial configurations. In order to obtain a potential from a chosen density, a discretized density profile is used, i.e.  $\rho(r)$  is held a constant over the radial bin defined around radius  $r$ . The calculation of the potential of a series of spherical mass shells is simple and is given in Paper I.

The only constraints placed on these trial functions is that the density profile is monotonically decreasing in radius and the DF is monotonically increasing in effective energy. Adherence to these conditions is demanded every time the profiles are altered to generate new profiles. Such tweaking of the functions takes place at the end of each iterative step.

At every iterative step, the current DF is projected into observable space, using the observed kinematical data. Thus, if we have information on the line-of-sight (LOS) velocity  $v_p$  and the apparent position  $r_p$ , then:

$$\nu_p(r_p, v_p) = \int dz \int \int dv_x dv_y f[v_r^2 + v_t^2 + 2\Phi(r)]. \quad (1)$$

Here  $r$  is the spherical radius and  $r_p$  the cylindrical radius on the plane of the sky, so that  $r_p^2 = x^2 + y^2 = r^2 - z^2$ ;  $v_r$  and  $v_t$  are components of velocity parallel and tangential to the radius  $\mathbf{r}$ . We choose the  $y$ -axis to lie completely in the plane containing the radius vector  $\mathbf{r}$  and the LOS. This implies that  $v_r^2 = (v_y \sin \theta)^2 + (v_z \cos \theta)^2$ ,  $\theta$  being the polar angle, i.e.,  $\cos \theta = z/r$ .

This projection of  $f(E)$  to  $\nu_p(r_p, v_p)$  could be achieved if a smooth approximation to  $f$  is considered. Another even simpler way (introduced in (Merritt 1996)) used in our work is to hold  $f$  a constant over any integral cell defined around a given value of  $E$ . Then corresponding to this energy bin, the projected distribution function is

$$\nu_p^{\text{cell}}(r_p, v_p) = \int dz A(r, r_p, v_p), \quad (2)$$

where  $A(r, r_p, v_p) = \int \int dv_x dv_y$  is the area that the energy bin occupies in phase space. Estimation of this area requires knowledge of the bounds on individual phase space coordinates that correspond to every energy bin. Identification of these bounds is discussed in Paper I. The total projected distribution function is a simple sum over all the energy bins, i.e.,

$$\nu_p(r_p, v_p) = \sum_i f_i \nu_{pi}^{\text{cell}}(r_p, v_p). \quad (3)$$

The product of all the projected distribution functions, each obtained for a pair of  $r_p$  and  $v_p$  in the observed data-set, gives a likelihood function  $L$ .

$$\log(L) = \sum_{i=1}^N \nu_{pi}, \quad (4)$$

where  $N$  is the total number of pairs of data points in the set and  $\nu_{pi}$  corresponds to the  $i^{\text{th}}$  data point.

When the accessible velocity data includes proper motion  $v_\mu$ , (where  $v_\mu = \sqrt{v_x^2 + v_y^2}$ ) rather than LOS-velocity data, the projection equation analogous to Eqn. 1 is:

$$\nu_\perp(r_p, v_\mu) = \int dz \int f(E) dv_z, \quad (5)$$

while if the data includes complete velocity information, the projection is simplest and is given by:

$$\nu_{3D}(r_p, v_\mu, v_p) = \int dz f(E). \quad (6)$$

The likelihood function is therefore a function in  $n$ -dimensions where  $n = n_r \times n_E$ . Here  $n_r$  is the number of radial bins corresponding to the chosen density profile and  $n_E$  the number of energy bins characterizing the DF. The global maxima of the highly non-linear function  $L$  is sought in this  $n$ -dimensional space by the Metropolis algorithm. A striking feature of using this method of optimization is that we are ensured a whole array or ensemble of models distributed according to the likelihood, rather than the single model associated with the maximum likelihood. The availability of the ensemble allows us to estimate uncertainties simply by measuring the spread of values across the ensemble. This is a big advantage of using the Metropolis algorithm. The maximization scheme is elaborated upon in Paper I.

Thus in CHASSIS, at the  $i^{\text{th}}$  iterative step, the DF and density profile are slightly tweaked from their forms used during the  $i-1^{\text{th}}$  step. The choice of these functions for the  $i^{\text{th}}$  step is referred to as  $\mathbf{x}_i$ . The current  $f$  is projected into observable space, at the currently chosen potential for each data point, and the likelihood for this step  $L(\mathbf{x}_i)$  is calculated. At the beginning Metropolis is expected to wander around in the multi-dimensional domain of the likelihood function and  $L$  tends to increase during this period. Soon, Metropolis settles down to an “equilibrium” phase during which the likelihood is likely to be close to the optimal value. Convergence is characterized in our code by the step  $k$  at which  $L(\mathbf{x}_k) < L(\mathbf{x}_{k-N_{\text{iter}}})$ . Here  $N_{\text{iter}} + 1$  is the total number of iteration steps that we use in any run. We recorded  $\mathbf{x}_{k-N_{\text{iter}}}, \dots, \mathbf{x}_k$  as our likelihood-weighted sample of  $\rho$  and  $f$ .

From the recorded DF and density profiles, mass within a pre-fixed radius  $r$  ( $M(r)$ ) is calculated as follows:

$$M(r) = \int_0^r \rho(r) 4\pi r^2 dr \quad (7)$$

In the discretized form, this equation is represented as:

$$M(r) = \frac{4\pi}{3} \left[ \delta^3 \sum_0^j \rho_i [3i^2 - 3i + 1] + \rho_j (r^3 - j^3) \right] \quad (8)$$

where  $r$  lies in the range  $[j\delta, (j+1)\delta]$ , i.e.  $j = \text{Integer}(r/\delta)$ .  $\delta$  is the width of a radial bin and  $j \in N$  such that  $j \leq \text{Integer}(r_{\text{max}}/\delta)$ .

The velocity dispersion profile  $\sigma(r)$  is calculated from the moments of  $f(E)$ .

$$\sigma(r)^2 = \frac{\int f(E) v^2 d^3\mathbf{v}}{\int f(E) d^3\mathbf{v}} - \left( \frac{\int f(E) v d^3\mathbf{v}}{\int f(E) d^3\mathbf{v}} \right)^2 \quad (9)$$

where  $v^2 = v_p^2 + v_\mu^2$  and  $E = v^2/2 + \Phi(r)$ . Thus, we obtain a value of  $\sigma(r_p)$  for every  $r_p$  in the

input data-set. This equation can be molded into the following difference equation:

$$\sigma(r)^2 = 2 \left[ \frac{3 \sum_0^j f_i \gamma_i^{5/2} (5i^4 - 10i^3 + 10i^2 - 5i + 1) - 3f_j(\Phi(r)^{5/2} - \gamma_j^{5/2})}{5 \sum_0^j f_i \gamma_i^{3/2} (3i^2 - 3i + 1) - 3f_j(\Phi(r)^{3/2} - \gamma_j^{3/2})} \right] - 2 \left[ \frac{3 \sum_0^j f_i \gamma_i^2 (4i^3 - 6i^2 + 4i^2 - 1) - 3f_j(\Phi(r)^2 - \gamma_j^2)}{4 \sum_0^j f_i \gamma_i^{3/2} (3i^2 - 3i + 1) - 4f_j(\Phi(r)^{3/2} - \gamma_j^{3/2})} \right]^2 \quad (10)$$

where

$$\gamma_i = \frac{\delta}{i} - \frac{\Phi}{i^2} \quad (11)$$

Here, the current energy is  $E_j$  that lies in the energy cell  $[j\delta, (j+1)\delta]$  i.e.  $j = \text{Integer}(E/\delta)$ .  $\delta$  is the width of an energy cell. Also,  $j \in N$  such that  $j \leq E_{max}/\delta$ , where the maximum value of energy used in the binning is  $E_{max}$ .

The error bars on the DF (and the density) are calculated at each energy-bin (or radial bin) as the difference between the DF (or  $\rho$ ) at the 84% level and that at the 16% level. However, the error bar on the value of velocity dispersion at any  $r_p$  is the difference between the value of the dispersion corresponding to the density at the 84% level and the value of  $\sigma(r_p)$  estimated with  $\rho(r_p)$  at the 16% level. This needs to be kept in mind when the dispersion results are examined.

The dispersion profile obtained in this manner is subsequently projected along the LOS and convolved with the density distribution to yield the LOS projected velocity dispersion profile which is a more realistic quantity from the point of view of observations. This projected velocity dispersion is then compared to the N-body profile.

#### 4. Implementation Details

The N-body realizations of the two clusters (Hyades and Arches) are used as inputs in CHASSIS to obtain the cluster density and DF of the constituent stars. The discretized density distribution is used to derive the cluster mass profile (Equation 8) and the DF recovered by the code is transformed to give us the velocity dispersion profile (see Equation 9). In the following sections, the enclosed mass and dispersion profiles of the N-body clusters are compared to those estimated by the inverse algorithm.

Testing of the code is reported in Paper I; the density and DF of a set of stars described by the Plummer model were calculated by the code. These quantities were found to match the Plummer density profile and DF quite well, within error bars.

Another important facet of any inverse algorithm is to confirm the independence of the results from the choice of the initial guess (which comprises of an arbitrarily chosen pair of DF and density profiles). We used very simple forms of density and distribution function as the initial guess in the

algorithm. The initial density function is given by:

$$\rho(r) = \rho_0 \left( 1 + \frac{r^2}{3r_c^2} \right)^\alpha, \quad (12)$$

where  $\rho_0$  is maintained a constant at 5000 and different choices of  $r_c$  and  $\alpha$  determine different initial density profiles. Changing  $\rho_0$  was found to have no bearing on the results while the results appeared most sensitive to the choice of  $\alpha$ . The effect of changing the initial density profiles was found to diminish with an increased number of iterative steps  $N_{\text{iter}}$ . At  $N_{\text{iter}}=4000$ , density profiles defined by  $\alpha$  lying in the range  $[-0.3, -3.5]$  and  $r_c \in [1, 7.5]$ , were found to imply similar results.

The initial DF has a normalization of unity and is chosen to have a simple power-law form.

$$f(\varepsilon) = (C + \varepsilon)^\beta, \quad (13)$$

where  $\varepsilon$  is the effective energy. A number of trial runs with different values of the constant  $C$  showed that the results are independent of it even with a relatively low  $N_{\text{iter}}$ . Thus we used  $C = 0$  in all our main runs.  $\beta$  on the other hand was a parameter that had greater effect on the results. We used initial DFs characterized by values of  $\beta \in [1, 10.5]$ . Any effect of the steepness of the initial choice of the DF on the results could be negated by using a large enough  $N_{\text{iter}}$  (4000 was found to suffice in the sense that the results were found to be consistent within the error bars).

## 5. Results from model H

The cluster properties that CHASSIS directly provides are the density and the equilibrium DF of the stellar sample selected from the N-body cluster. These cluster parameters are shown for the Hyades cluster in Figure 4. Since this data includes information on all three components of the velocity of each star, we use both LOS velocity as well as proper motion in our algorithm. Thus, the appropriate projection equation is given in Eqn. 6. The results obtained for this data-set are discussed below.

### 5.1. Independence from Initial Model

In this section we present evidence to establish the insensitivity of the results to the initial guess used in the algorithm. This is displayed via the concurrence of the enclosed mass and velocity dispersion profiles of the Hyades cluster, recovered by runs done with different initial guesses. For all these runs the input to the code constitutes of 37 stars, selected by their luminosity, from model H.

From Figure 5, we can see that changing the initial configuration results in profiles which agree with each other within error bars. This offers confidence about the robustness of the code insofar as changing the initial guess is concerned.



## 5.2. Number of data points

We conducted a series of numerical experiments to study the effect that the number of data points, used as inputs to the algorithm, has on the results suggested by the code. Samples of different sizes were selected by their luminosity, from the data-set corresponding to the N-body calculations that describe the Hyades cluster. The mass and velocity dispersion profiles of the cluster were calculated for these different input files and were compared to each other as well as with their N-body counterparts. One quantity that is of interest is the mass within the half-mass radius of the cluster. This is of course derived from the enclosed mass profile but being a simple scalar number, it can aid in gauging the extent to which the size of the input file is effective in determining results. The effect is shown in Figure 6. In addition to the value of the enclosed mass from different runs, the figure also depicts how well the predicted mass estimates tally with the N-body value.

The cluster profiles are shown in Figure 7.

The Figures 6 and 7 show that the number of stars for which kinematic information is fed into the algorithm, is not particularly influential in determining the mass profile accurately. It is however true in general that the errors in the calculation of the cluster parameters that are directly recovered by the code reduce with an increase in the input file size. This is discussed in Section 7.

## 5.3. Selection of Stars

A series of runs were undertaken to appraise the influence of the mode of selection of stars from the N-body realization of the cluster. The kinematic information of these chosen stars then form the input file for the inverse algorithm. One way to pick the stars from the N-body data set is to choose a certain number of stars at a random. Alternatively, we could sort the stars by their luminosity and accept the  $N$  brightest stars to form an input data file of size  $N$  (here  $N$  is any integer). We seek to explore the effect of these varying methods of building up the input data for CHASSIS.

In Figure 7, the enclosed mass and velocity dispersion profiles of the Hyades cluster, as predicted by the code are compared to the known (N-body) cluster configuration. The functions are obtained from runs done with input data files of diverse sizes, formed by choosing the constituent stars either randomly or by luminosity, from model H. The results show that when the stars are chosen by their luminosity, the match between the estimated and N-body quantities is in general better than when the choice is random. In fact Figure 7 indicates that CHASSIS does a good job in reproducing the cluster profiles when the stars are chosen by their luminosity. The results from the run done with the larger number of stars (199 stars) is particularly good. Even the run done with the much smaller number of stars (17) offers results that are consistent with the N-body mass profiles, within the error bars, which are indeed rather larger. However, the overlap between the velocity dispersion profile obtained from the latter run is not so good. One reason for this general

lack of agreement between the estimated velocity dispersion and the N-body dispersion profile is the shortcoming in the very method of extraction of the dispersion profile from the N-body data set. This is explained in details in Section 8.

## 6. Results from model A

N-body simulations of the Arches cluster gave us our model A. We have performed a number of runs with data selected from this model and fed into CHASSIS, in order to obtain the characteristics of the Arches cluster. Runs were implemented to evaluate the effect of changing the size of the input data set and of changing the manner of selecting stars from model A. The N-body simulation of this cluster has been performed at much lower radii compared to that of the Hyades cluster. One interesting difference between the two clusters is that the Arches cluster is identified as highly aspheric in the N-body calculations. Isotropy in velocity space is also a worse assumption for model A than model H. We have confined ourselves to the very central core of the Arches cluster (radius  $\leq 0.15\text{pc}$ ) where the effects of asymmetry in phase space are not too prominent (Figure 3).

Figure 8 shows the mass within the central  $0.093\text{pc}$  (the virial radius approximately), estimated by the code for input data sets of various sizes. This predicted value is compared to the N-body value of  $24,522M_{\odot}$  of the enclosed mass.

The effect of the process of selecting the stars from the N-body realization of the Arches cluster is displayed in Figure 9. The figure shows the cluster profiles obtained from a number of runs which are performed with differently sized input files that were constructed by picking stars randomly from model A. From these runs, it is clear that the inverse algorithm over-estimated the enclosed mass at larger radii. When the stars are chosen in decreasing order of their luminosity, the runs show better match with the N-body mass profiles, within error bars. The compatibility with the known velocity dispersion profiles was likewise poorer for these runs.

## 7. Discussions

The aim of this paper was to advance the case of using CHASSIS to characterize stellar clusters. We proceeded in this exercise by first introducing the reader to the salient features of the inverse algorithm CHASSIS. This was followed by testing the code with simulated kinematical data for two different clusters, Hyades and Arches.

The signatures of the clusters, as known via the N-body simulations were compared to the characteristics recovered by the code. The degree of overlap between the simulated cluster configurations and the predicted ones is expected to shed light on the applicability of the algorithm. The relevant cluster attributes were judged to be the enclosed mass and the line-of-sight projected velocity dispersion profiles.

We tested the robustness of the algorithm to variations in the initial guess for the cluster characteristics (see Figure 5). Results were compared from runs done with the steepness of the initial density profile varying from  $\alpha = -1.5$  to  $-2.5$  and  $-3.5$  at a fixed choice of the initial DF. The recovered mass profiles agreed with each other very well within error bars (as well as with the N-body profile). Similarly promising results were obtained from runs done with a fixed initial density profile and a DF which varied in steepness ( $\beta$  was changed from 5.5 to 6.5 and 7.5). In regard to the velocity dispersion profiles, it is seen that the overall match is good though when seen over short length scales, the degree of overlap is not as good as it is in the case of the mass profiles. This is in fact a feature that is consistently borne by all the presented velocity dispersion profiles.

This discrepancy owes more to the way the known dispersion is drawn out from the N-body simulations of the clusters than on the calculation of the dispersion by CHASSIS. The projected radii from the N-body data sets are binned and the velocities of the stars in each such bin is calculated. (For model H, stars with velocities lower than  $1\text{kms}^{-1}$  were used in this calculation while for the Arches cluster, stars in each bin with velocities lower than  $20\text{kms}^{-1}$  were used). This discrete distribution of velocity dispersions is plotted in Figure 10 as crosses. This distribution is “optimally” smoothed to represent the velocity dispersion of the cluster. By “optimal” smoothing is meant smoothing done (using the SuperMongo software) with a filter size which if exceeded renders the plot less jagged but does not alter the overall shape. This smoothed run of the dispersion with  $r_p$  is what the calculated (by CHASSIS) dispersion profile is compared to. This method of extracting the dispersion profile from the N-body results is indeed *ad hoc* to some extent but the methodology is adopted consistently; consequently, for the purposes of comparison, it is good enough.

There is another technical reasons why in general the match between the calculated and known velocity dispersion profiles is less good than that between the enclosed mass profiles. The mass profile of the relevant cluster is estimated from its density via Equation 8 while velocity dispersion is calculated using Equation 9. Since the latter equation involves two summations unlike only one in Equation 8, it is expected that any error in the estimation of the DF will imply greater deviation in the evaluated dispersion value than any error in the estimated density will contribute to the mass profile.

The quantities that the inverse algorithm directly offers are the density profile and the equilibrium distribution function of the set of stars for which kinematical data is used as input to the code. These quantities were then used to calculate the mass and dispersion profiles, under the assumptions of sphericity and isotropy in velocity space. These assumptions were essentially made to ease our calculations but are not necessarily realistic constraints on clusters. For example, we recognize the Arches cluster as highly aspheric from the N-body simulations. In order to be able to predict stable results with CHASSIS, we confined our analysis to radii within which the degree of asphericity and anisotropy is markedly low.

The way to ensure that the set of stars which is used as input to CHASSIS is closer to a spherical configuration is by using the kinematical data of the more massive stars. These stars form a subset

in the cluster that is relatively more spherical. It is after all the tidal field of the Galaxy, which when included in the N-body simulations, causes the cluster to elongate in one direction. This field has a weaker effect on the heavier than the less massive stars in the cluster since the more massive stars tend to reside closer to the center of the cluster owing to mass segregation. This is confirmed by Figure 11: the left panel in this figure represents the run of the ratio of the transverse to the radial velocity component of 200 stars chosen from model A. In one case the stars are chosen by luminosity (results depicted in unfilled circles) while in the other case they are chosen randomly (filled triangles). The distribution of the ratio  $v_\mu/v_z$  with  $r_p$  is more centrally concentrated when the more massive (i.e. roughly speaking the brighter stars) are included in the sample – there are comparatively more triangles at higher radii. The right panel of the same figure shows that the effect of the tidal field of the Galaxy is more pronounced in the sample constructed via random selection of the stars. The value of apparent position is indexed by a number in the data set representing the sample; the ratio  $r_p/z$  is plotted against this number for the two samples. The distributions of the ratios are smoothed by the same amount in both cases and show that the sample of stars constructed by random choice is less spherical than when the choice is by mass.

In this context, let us reiterate that the choice on the basis of stellar mass roughly resembles the choice based on luminosity. In fact, a few runs were carried out with the  $N$  most massive stars and the profiles obtained from these runs corroborated the results already mentioned.

Thus, if the input set of  $N$  stars ( $N$  is a natural number) is formed by choosing the  $N$  most massive stars within a certain radius, instead of choosing  $N$  stars randomly, the assumption of sphericity is more closely obeyed and the enclosed mass profile as recovered by CHASSIS is expected to be more compatible with the N-body profile. In fact this is true even interior to the radial cutoffs that we have imposed in our selection of the stars from the N-body outputs (of 10pc and 0.15pc for the Hyades and Arches clusters respectively), as verified by Figure 11.

If the set of stars used as input to the algorithm form an aspherical configuration, then it is to be expected that our code will over-estimate the mass, (see Figure 12). This is what is seen from runs done with input data sets that are formed by choosing stars randomly. This is evident in the lower panels in Figure 7 and Figure 9;

We have also explored the effect of changing the number of data points ( $N$ ) which are used as input to the code. Naively, one may conclude that a larger number of data points invariably improves the result in the sense that the error-bars diminish in size. The larger the data set, the narrower is the region around the maximum of the likelihood function in the multi-dimensional energy-radius space. Consequently, the wandering of the Metropolis algorithm in its “equilibrium” phase is smaller, thus bringing down the extent of the errors. Albeit it is expected that increasing the number of input data points is soon going to lead to nearly stable results.

It is noticed that until the number of stars in the input data set is about 80, the simulated and predicted quantities are closer for the Hyades cluster than when the Arches cluster is used (see Figure 7 and Figure 9). One reason for this is that the Arches cluster is known from the N-body

simulations to be much more aspheric than the Hyades. The degree of anisotropy in velocity space is also greater in Arches. As stated in Section 2, even in the central 0.15pc, the ratios of the different components of the velocity (and spatial) dispersion, when sought as functions of radius, undulate about a mean of unity. The same quantities for the Hyades cluster are less non-linear inside the chosen radial cutoff for model H (about 10pc). Thus, for the Arches cluster, stability in the results is attained at a higher value of  $N$  (at about  $N = 80$ ) than when input data is chosen from model H for which this number is 17. This is evident in the comparison of Figures 6 and 8.

Our code is rather powerful in the sense that it can spot the answers even when  $N$  is quite low. We propose that this potency is a direct outcome of implementing the Metropolis algorithm as the optimizer. Metropolis is a highly competent algorithm and is more effective than when the maxima in the likelihood function is sought by brute force as in other non-parametric projects that have used an isotropic distribution function (Merritt & Saha 1993; Merritt & Tremblay 1993). When the likelihood is highly non-linear, such a method is not strong enough to recover the maximal region of the likelihood unless the number of input data points is sufficiently high to adequately constrain the likelihood. Even when Metropolis is used, we find that for a model such as model H, we need to have around 100 data points to constrain the enclosed mass at the half-mass radius within a range of about  $120M_{\odot}$ , i.e. fractional errors of about 20%.

The approximation of isotropy, as used in the algorithm, aids in simplifying the calculations but needs to be improved via the inclusion of a two-integral distribution function in the code. This is planned as a future exercise.

## 8. Conclusions

We have carried out analysis of two N-body clusters using the inverse algorithm, CHASSIS. Our code aims to simultaneously recover the potential and the distribution function of the stars whose kinematic details are fed in as input. The global maxima in the likelihood function is sought by the Metropolis algorithm. The cluster profiles directly offered by the algorithm are used to calculate the line-of-sight projected velocity dispersion and enclosed mass profiles of the cluster.

We looked into the robustness of the code with respect to change in the used initial parameters. The nearly concurrent results reflect that the code does indeed withstand variations in the input configurations very well (see Figure 5).

When input data was used from the model that mimics the Hyades cluster, the enclosed mass and the velocity dispersion profiles predicted by the code were consistent with the simulated profiles for the Hyades cluster as long as the number of kinematic data points used as input in the code is at least 17 though the error bars that accompany the results from this run are very large. For the Arches cluster, an input data set with at least as many as 63 stars is required to yield a mass profile that is consistent with the N-body profile within the error bars though the velocity dispersion profile from this run falls short of the predicted N-body dispersions (Figure 9). The input data set

needs to contain kinematic information of at least 80 stars to result in both mass and dispersion profiles that are compatible with the known profile, within the error bars.

The overlap between the quantities suggested by the code and the N-body profiles is better when the input model follows the assumption of phase space isotropy closely, i.e. within about 10pc for the Hyades and 0.15pc for the Arches cluster.

When the input file comprises the brightest stars, the predictions of the code match the cluster profiles better than when the stars are picked randomly. Roughly speaking, the brightest stars tend to follow the trend of the most massive stars and are segregated toward the cluster center while the dimmer stars are more prominent in the cluster halo. Thus, the observer who is likely to look toward the center stands a greater chance of picking out those stars for which the code predicts the correct results. Consequently, CHASSIS can claim to be a propitious tool for the analysis of data of stellar clusters.

Increasing the number of stars in the input file does not affect the results beyond decreasing the size of the error bars; for a given model, there is a minimum value of this number, which when exceeded implies stable results. This value is low when the cluster is very nearly spherical and isotropic. For the Arches cluster this numerical value is around 80 while it is as low as about 17 for the Hyades cluster though the run done with these 17 stars yields very large error bars; at the half-mass radius of the N-body model for the Hyades cluster, the mass enclosed varies in the range of about  $500M_{\odot}$  to  $900M_{\odot}$ . (As  $N$  increases, the error bars reduce in size considerably, so that when  $N \sim 200$ , the mass within the half-mass radius ranges from about  $582M_{\odot}$  to about  $586M_{\odot}$ ). We believe that is it our sophisticated optimization routine that utilizes the Metropolis algorithm that helps us to identify the correct answers even with quite small input data sets. The search for the range of  $N$  that corresponds to consistent results can be fully automatized.

Our numerical experiments offer confidence in the applicability of CHASSIS as a tool to analyze stellar clusters. The algorithm has been shown to be successful when the cluster is spherical and isotropic in velocity space. The assumption of isotropy is an ingredient in the code which is under review.

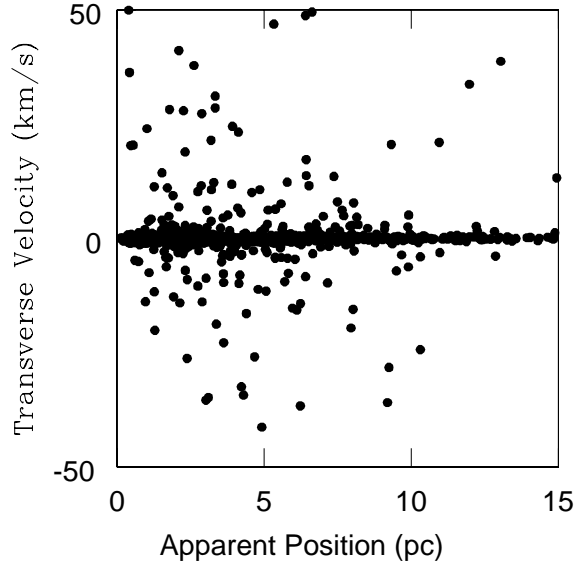
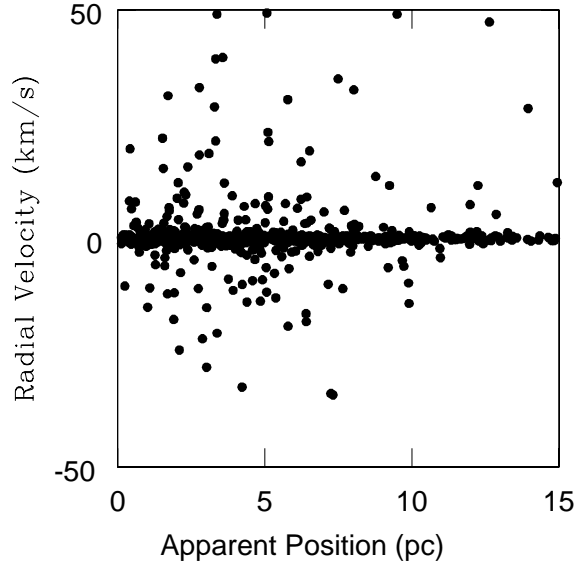
CHASSIS has been used previously to estimate the mass of the central black hole in the Galaxy (Paper I) and in this paper, to characterize open stellar clusters. In its present form, it is put forward as a useful tool to understand kinematic data of other stellar systems such as clusters.

### Acknowledgments

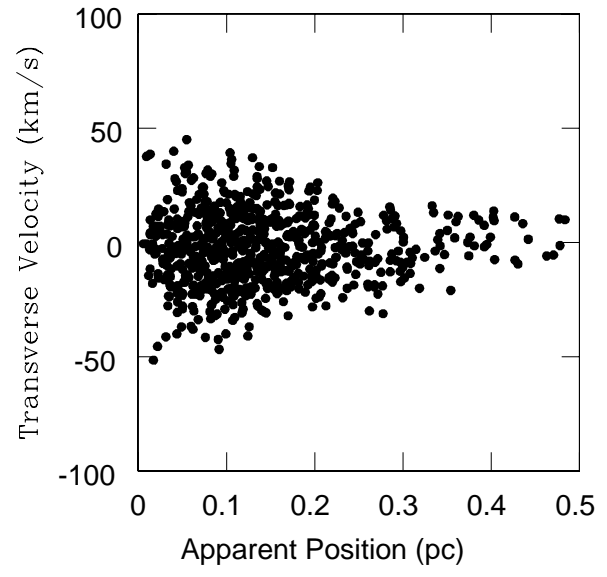
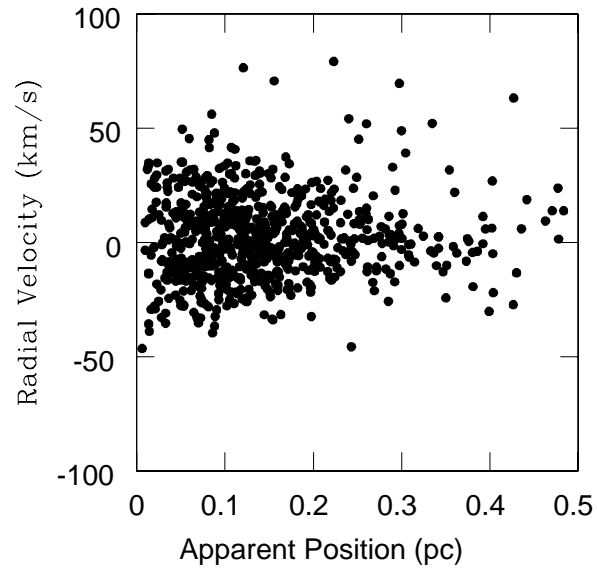
DC would like to acknowledge Dr. P. Saha who is the joint author of CHASSIS. SPZ was supported by the Royal Dutch Academy of Sciences (KNAW) and by the Netherlands Organization of Scientific Research (NWO). We would also like to thank the anonymous referee whose careful scrutiny helped to improve the paper considerably.

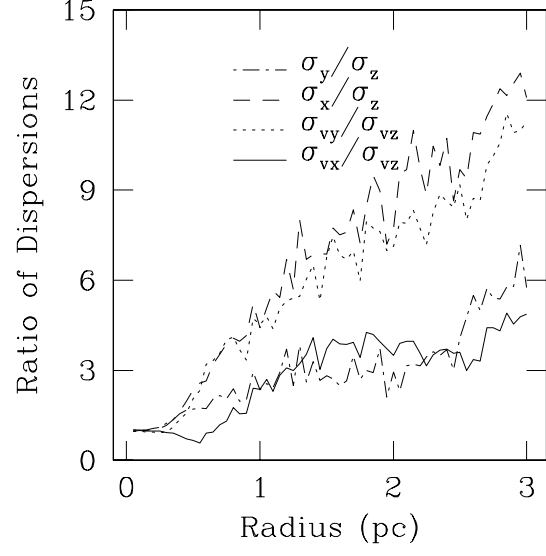
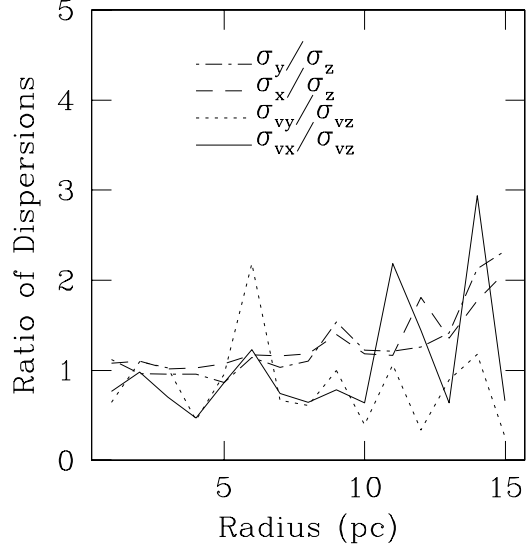
Table 1: Initial and final conditions for the N-body models of the Arches and Hyades clusters. Columns give the initial density profile (King 1966 model parameter), the number of stars, the total cluster mass (in  $M_{\odot}$ ), the virial radius (in parsec) and the tidal radius of the cluster and its distance to the Galactic center. The subsequent columns give the parameters for these models at the moment the data was analyzed by the inverse algorithm; the time (in Myr), the number of remaining stars bound to the cluster, the total mass of these stars (in  $M_{\odot}$ ), the half mass radius and the distance to the Galactic center.

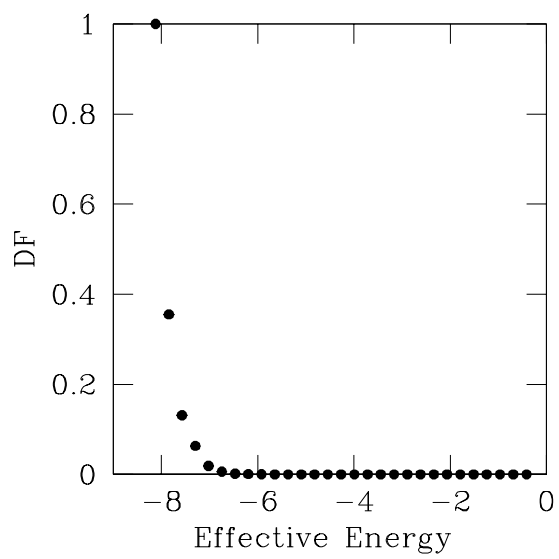
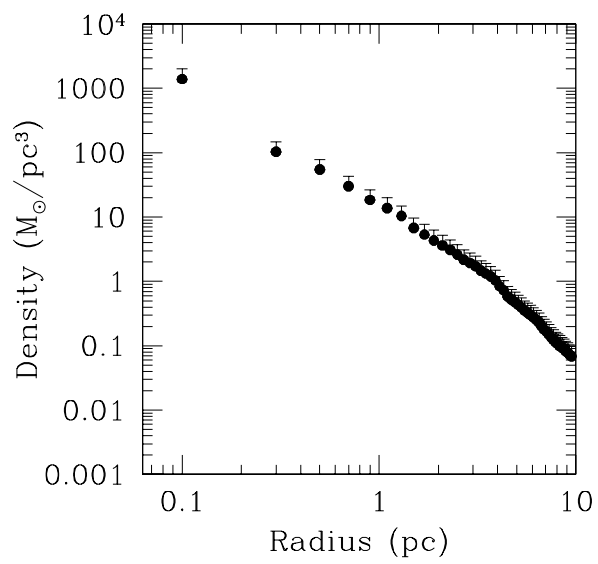
Name	Wo	N	M ( $M_{\odot}$ )	Rhm (pc)	Rt (pc)	Rgc (pc)	T (Myr)	N	M ( $M_{\odot}$ )	Rhm (pc)	RGC (pc)
A	3	64k	62600	0.17	0.52	6.0	0.97	55224	54200	0.093	2.8
H	6	3k	1606	2.50	13.7	13k	400	2628	1192	4.66	13k

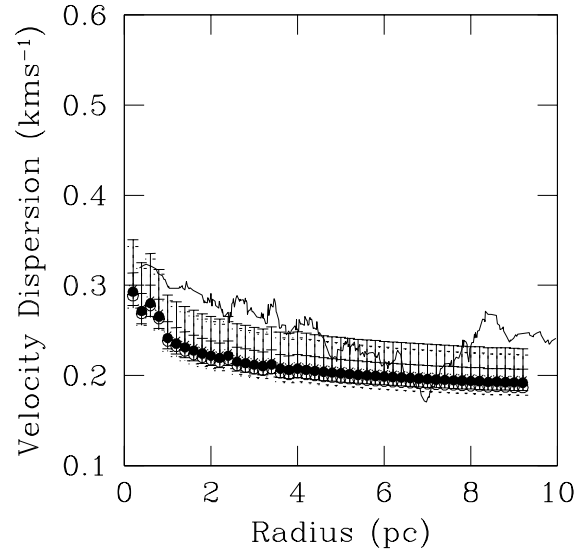
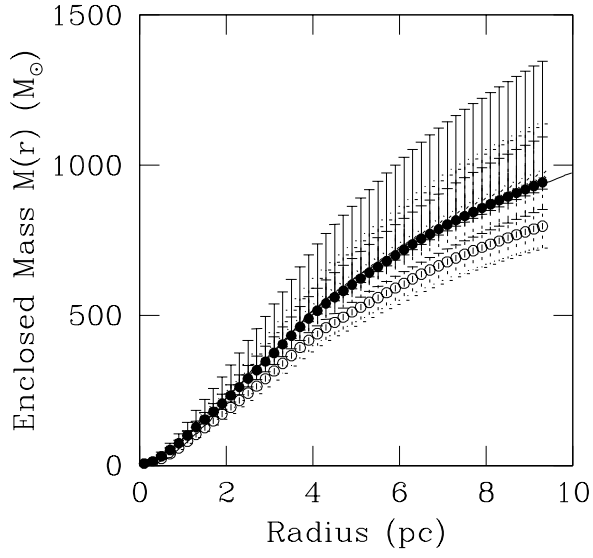
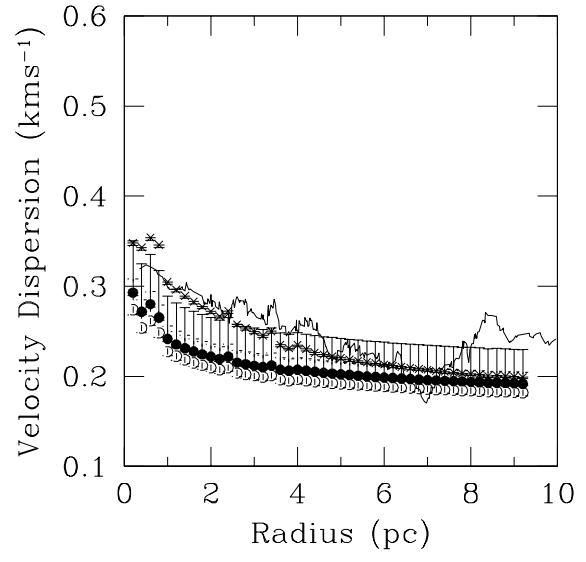
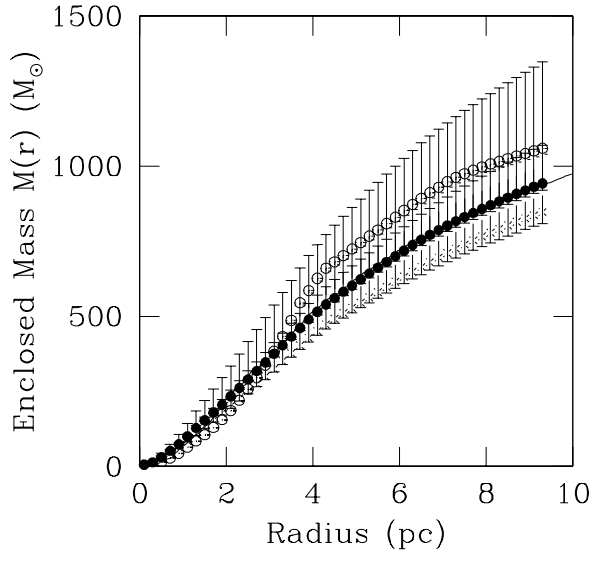


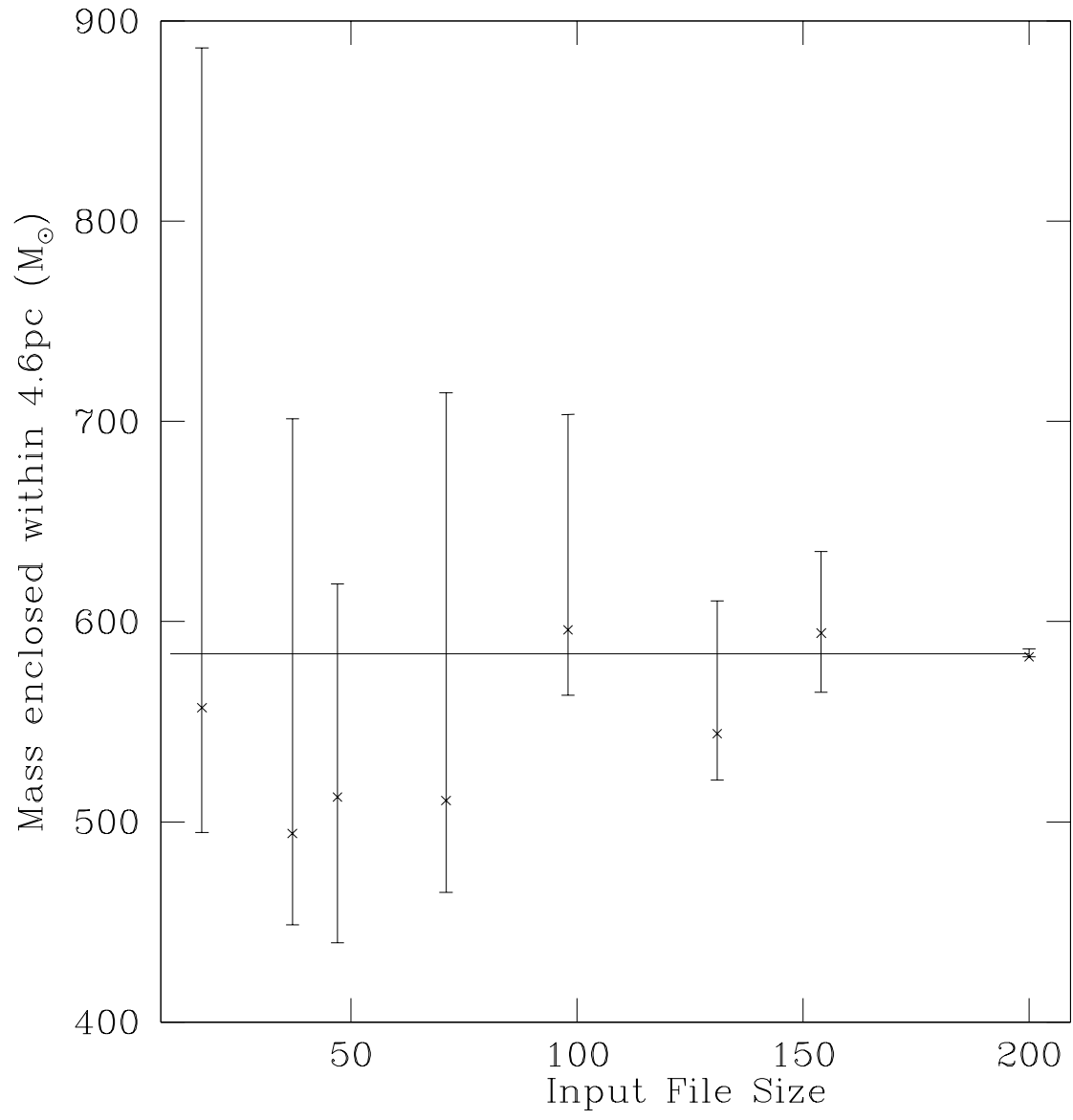


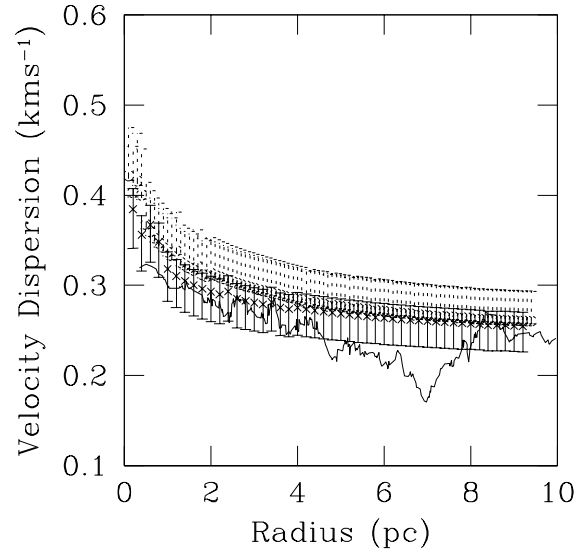
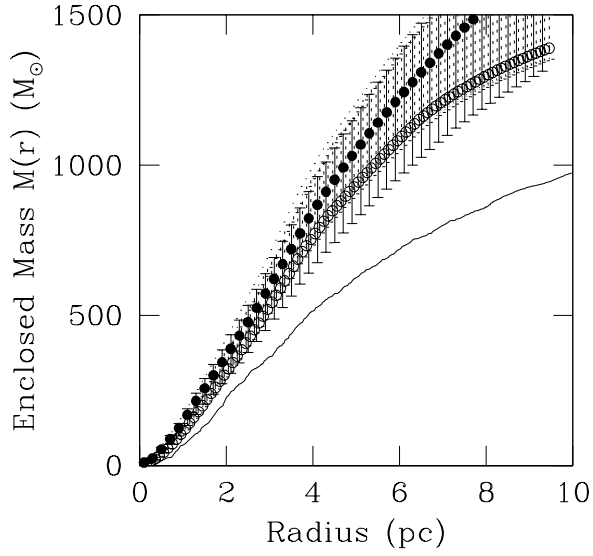
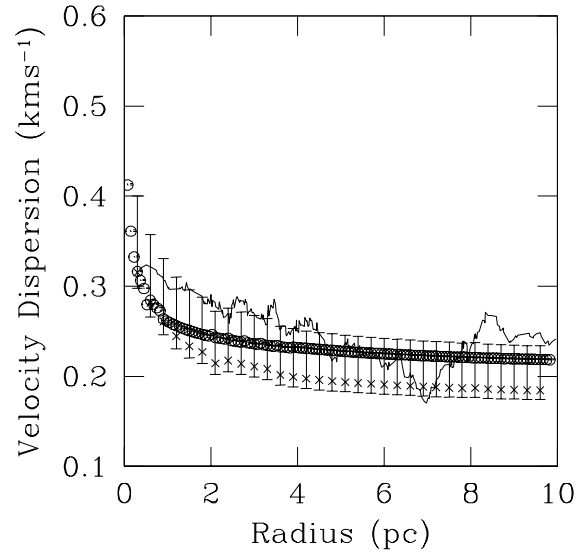
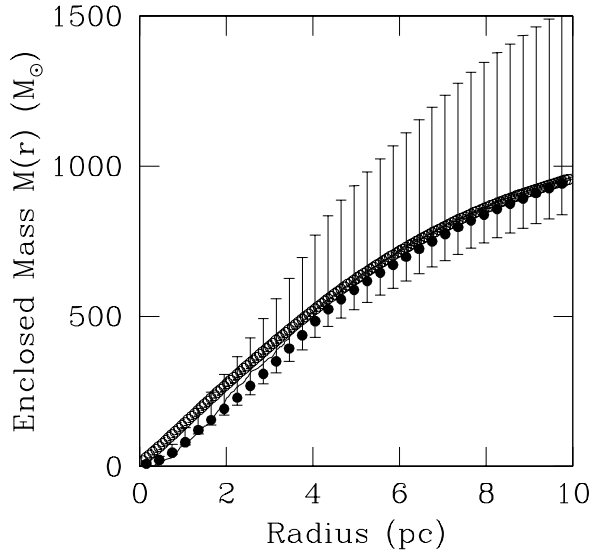


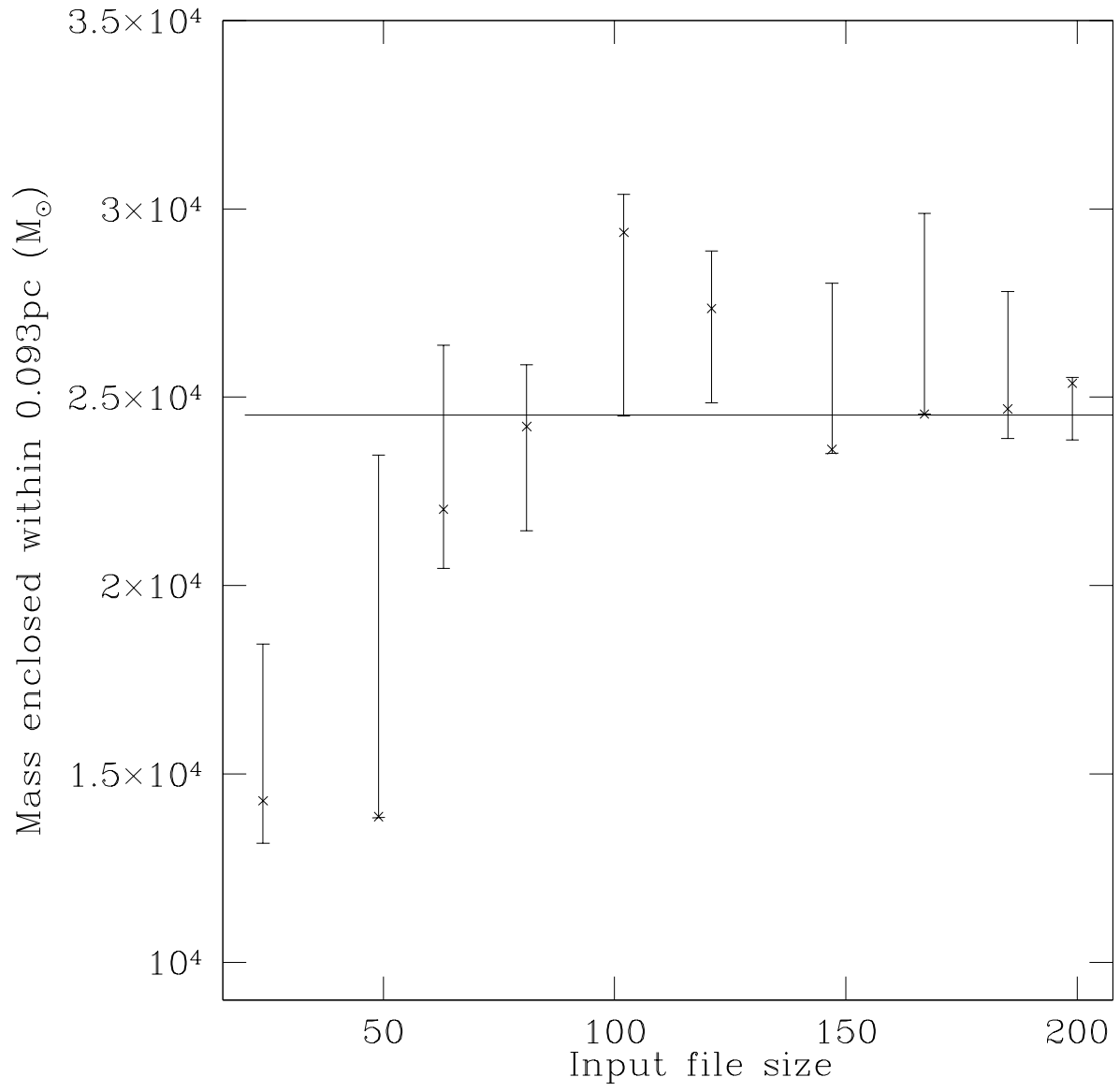


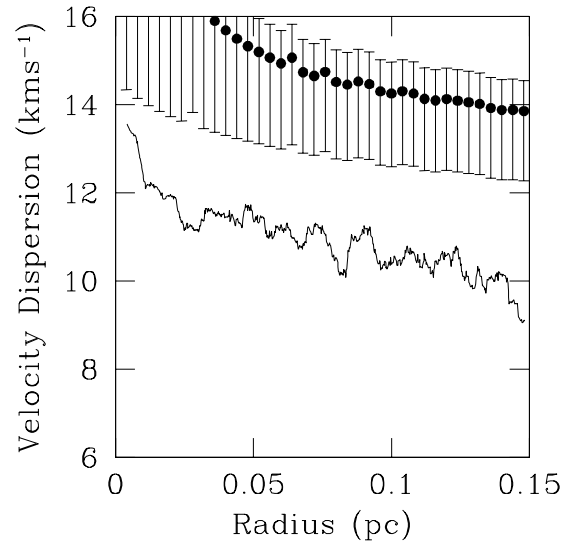
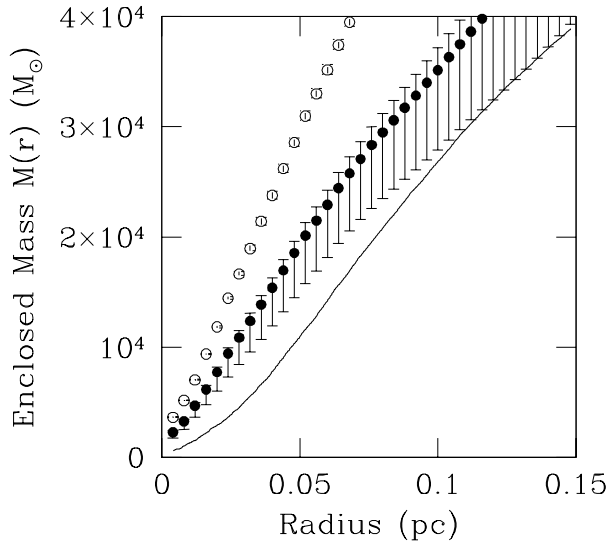
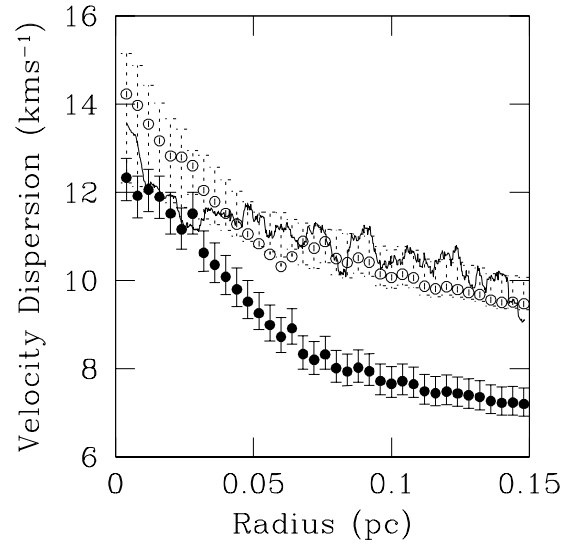
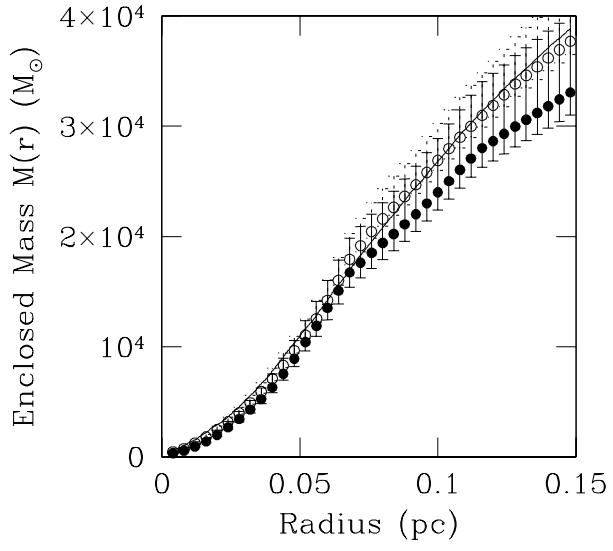




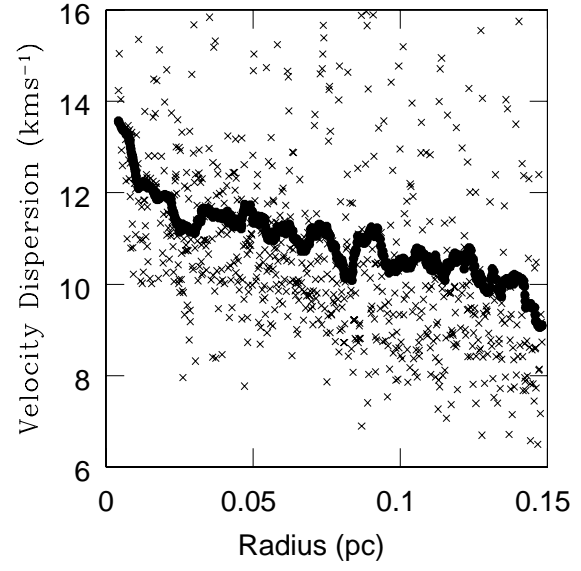
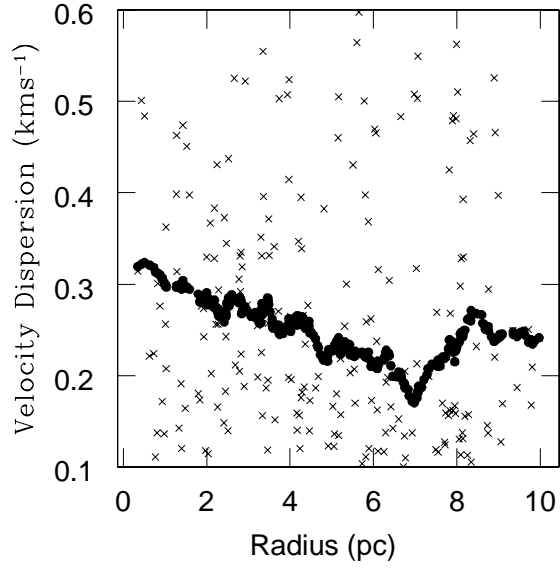


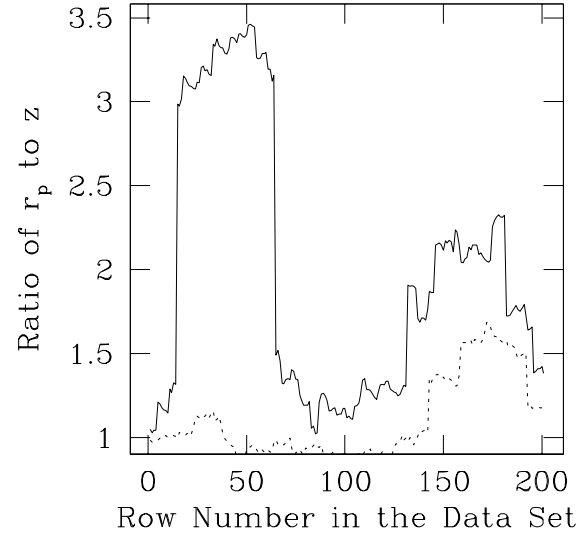
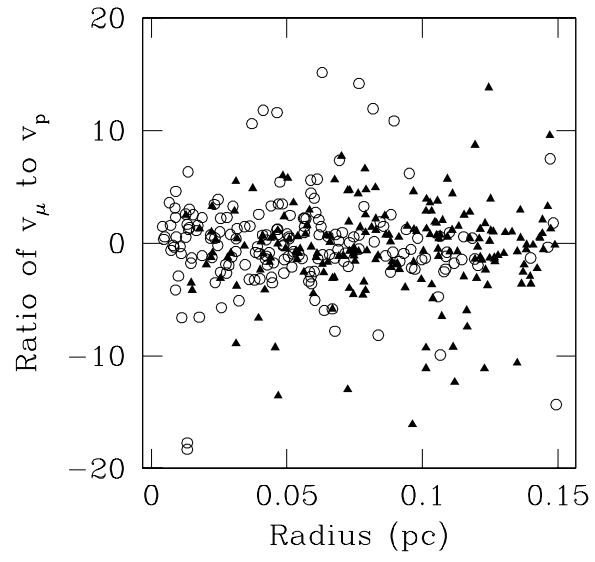


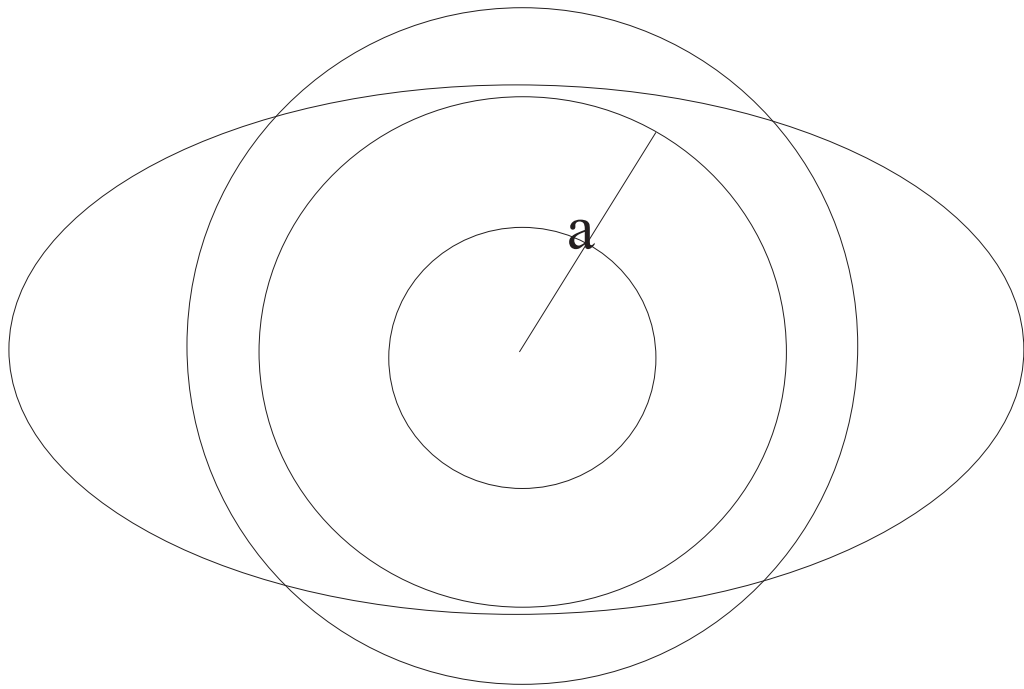












## REFERENCES

- Larsen, S.S., Brodie, J., Elmegreen, G., Efremov, Y.N., Hodge, P.W., and Richtler, T., 2001, *ApJ*, 556, 801.
- Merritt, D., and Tremblay, B., 1993, *AJ*, 106, 2229.
- Merritt, D., and Saha, P., 1993, *AJ*, 409, 75.
- Genzel, R., Thatte, N., Krabbe, A., Kroker, H., and Tacconi-Garman, L. E., 1996, *ApJ*, 472, 153.
- Bosch, G., Selman, F., Melnick, J., and Terlevich, R., 2001, *A&A*, 380, 137.
- Ghez, A. M., Klein, B. L., Morris, M., and Becklin, E. E., 1998, *ApJ*, 509, 678.
- Chakrabarty, Dalia, and Saha, P., 2001, *AJ*, 557, 292 (Paper I).
- Merritt, D., 1996, *AJ*, 112, 1085.
- Portegies Zwart, S.F, Makino, J., McMillan, S.L.W., and Hut, P., 2002, *ApJ*, 565, 265.
- Portegies Zwart, S.F, McMillan, S.L.W., Hut, P., and Makino, J., 2001, *MNRAS*, 321, 199.
- Makino, J., Taiji, M., Ebisuzaki, T., and Sugimoto, D., 1997, *ApJ*, 480, 432.

Fig. 1.— Plots of radial (left panel) and transverse (right panel) velocities of stars in model H against apparent positions. The data is obtained from N-body calculations described in the Section 2. To construct this plot, we have chosen every  $3^{rd}$  star in the N-body representation of this cluster.

Fig. 2.— Plots of radial and transverse velocities of stars in model A, against apparent position. This N-body cluster has 55,224 stars in it but only stars at pre-fixed intervals in projected radius have been included in the plot.

Fig. 3.— Ratio of the  $x$  and  $y$  components of the velocity (and spatial) dispersion,  $\sigma_{vx}$  and  $\sigma_{vy}$  (and  $\sigma_x$  and  $\sigma_y$ ) to the  $z$  component of the velocity (an spatial) dispersion,  $\sigma_{vz}$  (and  $\sigma_z$ ).

Fig. 4.— Figure showing the density (left panel) and equilibrium stellar distribution function (right panel) of the Hyades cluster, as recovered from a run done with the initial configuration given by  $\alpha = -1.5$  and  $\beta = 5.5$ , using an input file of 37 randomly picked stars from model H. The error bars are at the 16% and the 84% levels.

Fig. 5.— Profiles of the Hyades cluster, as estimated by CHASSIS, from runs performed with various initial configurations. The left panels display the enclosed mass profiles while the velocity dispersion profiles recovered from the different runs are shown in the right panels. In the upper panels, the index  $\beta$  is held a constant (at 5.5) and  $\alpha$  is changed. The profile for  $\alpha = -1.5$  is marked by error bars in solid lines with superimposed filled circles at the 50% level, those for  $\alpha = -2.5$  are in dotted lines with open circles and for  $\alpha = -3.5$  errors are in dashed lines with crosses. In the lower panels the initial density profile is maintained the same ( $\alpha = -1.5$ ) but the initial choice of the DF varies in steepness.  $\beta = 5.5, 6.5$  &  $7.5$  are marked by error bars in solid, dotted and dashed lines, superimposed with filled circles, open circles and crosses respectively. The results obtained from the calculations of the data describing model H are shown in solid black lines. The error bars are at the 16% and the 84% levels. In the dispersion profiles, the error bar at any radius is calculated as the difference between the dispersion value corresponding to the value of density at the 84% level and at the 16% level. The input for the algorithm is the set of the 37 brightest stars in model H.

Fig. 6.— Figure showing the estimates of mass enclosed within the inner 4.6pc in model H (the half-mass radius), indicated by CHASSIS, from runs done with input data of a varying number of stars, selected by their luminosity. The mass estimates are shown with superimposed error bars (at the 16% and 84% levels). The N-body calculations imply a mass of about  $584M_{\odot}$  of the cluster. This value is represented by a solid line.

Fig. 7.— Figure showing the enclosed mass and velocity dispersion profiles of Hyades, as claimed by CHASSIS from runs done with input data that has either been picked randomly (lower panels) or according to the luminosity of stars (upper panels). When the stars are sorted by their luminosity, the  $N$  most luminous among them are selected from model H, where  $N$  is an integer. For  $N=17$ , the error bars are in solid lines superimposed with filled circles (to mark the 50% level) while they

are shown in dotted lines with open circles for  $N = 199$ . When the stars are picked randomly, the match is comparatively worse. Two values of  $N$  are used for these runs; profiles are shown with errors in solid lines superimposed with filled circles for  $N = 37$  and dotted lines with open circles for  $N = 71$ . The curve in solid line represents the profiles indicated by the N-body calculations.

Fig. 8.— Similar to Figure 6 except that here the mass enclosed within the inner 0.093pc of the Arches cluster (half-mass radius) is displayed. The mass estimates are from runs done with input files of various sizes, constructed by picking stars by their luminosity from model A. The N-body estimate of the mass within this radius is about  $24,522M_{\odot}$ . This value is represented by the solid black line.

Fig. 9.— Similar to Figure 7 except that here the profiles of the Arches cluster are shown. When the input file size  $N$  is 63 the error bars are in solid lines and the symbol type at the 50% mark is filled circle while these are dotted lines and open circle respectively for  $N = 185$ . In the lower panels, for  $N = 17$  the error bars are in solid lines, superimposed with filled circles while the same are in dotted lines and open circles for  $N = 200$ .

Fig. 10.— Figure showing the discrete distribution of velocity dispersion values with radius. At each (projected) radial bin, the raw stellar velocities from the output of the N-body simulations are used to calculate the velocity dispersion in that bin. These are plotted as crosses against projected radius. An optimally smoothed curve is fit to this distribution of points. By “optimal” is implied that size of the smoothing filter which if exceeded helps to reduce the unevenness of the plot but retains the overall shape of it. This velocity dispersion plot obtained from the N-body model is compared to the LOS projected dispersion estimated by CHASSIS.

Fig. 11.— Figure showing the effects of choosing stars randomly as distinguished from building a sample by selecting the most massive (i.e. roughly speaking, the brightest) stars. In the left panel, the ratio of the transverse ( $v_{\mu}$ ) to the radial ( $v_p$ ) velocity of 200 stars in the sample, is plotted against projected radius. When the choice is random, the result is shown in filled triangles while selection by luminosity is represented by open circles. The position of a value of  $r_p$  in the data set is indexed by a row number; the ratio  $r_p/z$  is plotted against this number in the right panel. The results are equally smoothed for the two samples. The distribution of the ratio is in broken lines when the selection is by mass and is in solid lines when the choice is random.

Fig. 12.— Figure to show why we should expect our algorithm to overestimate the enclosed mass in an aspheric cluster, at higher radii. The ellipse represents the 2-D projection of a perfectly oblate cluster. Within radii  $R \leq a$  the enclosed mass is correctly calculated by the code. A fraction of any annulus at  $R < a$  lies outside the cluster. Now, the code uses the density in the shell at any radius, to spread the mass uniformly throughout that annulus. Thus, the mass estimated to lie inside the annulus at radii  $> a$  is in excess of the actual mass enclosed within this radius.